Hum Genet (2015) 134:181–190
DOI 10.1007/s00439-014-1509-2

ORIGINAL INVESTIGATION

Characterization of *ANKRD11* mutations in humans and mice related to KBG syndrome

Katherina Walz · Devon Cohen · Paul M. Neilsen · Joseph Foster II. · Francesco Brancati · Korcan Demir · Richard Fisher · Michelle Moffat · Nienke E. Verbeek · Kathrine Bjørgo · Adriana Lo Castro · Paolo Curatolo · Giuseppe Novelli · Clemer Abad · Cao Lei · Lily Zhang · Oscar Diaz-Horta · Juan I. Young · David F. Callen · Mustafa Tekin

Received: 10 October 2014 / Accepted: 9 November 2014 / Published online: 21 November 2014

Abstract Mutations in *ANKRD11* have recently been reported to cause KBG syndrome, an autosomal dominant condition characterized by intellectual disability (ID), behavioral problems, and macrodontia. To understand the pathogenic mechanism that relates *ANKRD11* mutations with the phenotype of KBG syndrome, we studied the cellular characteristics of wild-type ANKRD11 and the effects of mutations in humans and mice. We show that the abundance of wild-type ANKRD11 is tightly regulated during the cell cycle, and that the ANKRD11 C-terminus is required for the degradation of the protein. Analysis of 11 pathogenic *ANKRD11* variants in humans, including six reported in this study, and one reported in the *Ankrd11*$^{Yod/+}$ mouse, shows that all mutations affect the C-terminal regions and that the mutant proteins accumulate aberrantly. In silico analysis shows the presence of D-box sequences that are signals for proteasome degradation. We suggest that ANKRD11 C-terminus plays an important role in regulating the abundance of the protein, and a disturbance of the protein abundance due to the mutations leads to KBG syndrome.

K. Walz and D. Cohen contributed equally to this work.

Electronic supplementary material The online version of this article (doi:10.1007/s00439-014-1509-2) contains supplementary material, which is available to authorized users.

K. Walz (✉) · D. Cohen · J. Foster II. · C. Abad · C. Lei · L. Zhang · O. Diaz-Horta · J. I. Young · M. Tekin (✉)
Dr. John T. Macdonald Foundation Department of Human Genetics and John P. Hussman Institute for Human Genomics, Miller School of Medicine, University of Miami, 1501 NW 10 Ave, BRB 610, M-860, Miami, FL 33136, USA
e-mail: kwalz@med.miami.edu

M. Tekin
e-mail: MTekin@med.miami.edu

K. Walz
Department of Medicine, Miller School of Medicine, University of Miami, 1501 NW 10 Ave, BRB 418, M-860, Miami, FL 33136, USA

P. M. Neilsen · D. F. Callen
Swinburne University of Technology Sarawak Campus, Kuching, Sarawak, Malaysia

F. Brancati
Department of Medical, Oral and Biotechnological Sciences, Gabriele D'Annunzio University, 66100 Chieti, Italy

Introduction

Heterozygous mutations in *ANKRD11* (MIM611192), encoding ankyrin repeat domain 11, have recently been

F. Brancati · G. Novelli
Medical Genetics Unit, Policlinico Tor Vergata University Hospital, Viale Oxford 81, 00133 Rome, Italy

K. Demir
Division of Pediatric Endocrinology, Dokuz Eylül University Faculty of Medicine, İzmir 35340, Turkey

R. Fisher
Northern Genetics Service Teesside Genetics Unit, The James Cook University Hospital, Marton Road, Middlesbrough TS4 3BW, UK

M. Moffat
Department of Paediatric Dentistry, Newcastle Dental Hospital and School, Richardson Road, Newcastle upon Tyne NE2 4AZ, UK

N. E. Verbeek
Department of Medical Genetics, University Medical Center Utrecht, Lundlaan 6, 3584 EA Utrecht, The Netherlands

shown to cause KBG syndrome (MIM148050), characterized by intellectual disability (ID), behavioral abnormalities, macrodontia of upper central incisors, and skeletal anomalies (Brancati et al. 2006; Herrmann et al. 1975; Skjei et al. 2007; Sirmaci et al. 2011). Heterozygous deletions at 16q24.3 that contain the *ANKRD11* gene were also described in patients with ID, autistic spectrum disorder, and in some cases with brain anomalies, a clinical phenotype overlapping with KBG syndrome (Marshall et al. 2008; Willemsen et al. 2010; Handrigan et al. 2013; Isrie et al. 2012; Sacharow et al. 2012; Khalifa et al. 2013; Miyatake et al. 2013).

ANKRD11 contains two transcriptional repression domains at the N and C termini, respectively, plus a transcriptional activation domain (Zhang et al. 2007). It interacts with the p160 coactivator and nuclear receptor complex and recruits histone deacetylases to modify transcriptional activation (Zhang et al. 2004). ANKRD11 localizes mainly to the nuclei of neurons and accumulates in discrete inclusions when neurons are depolarized (Sirmaci et al. 2011). Thus, it is not surprising that *ANKRD11* mutations lead to a neurobehavioral phenotype (Willemsen et al. 2010; Handrigan et al. 2013; Sacharow et al. 2012; Spengler et al. 2013). However, how *ANKRD11* mutations act at the molecular level remains unknown.

The mouse ortholog Ankrd11 has a 79 % identity at the amino acid level with human ANKRD11. A chemically induced (ENU) mutagenesis screen generated the *Ankrd11*$^{Yod/+}$ allele, a missense mutation at a highly conserved residue (E2502K) (Barbaric et al. 2008). The *Ankrd11*$^{Yod/+}$ or *Yoda* mouse was reported before the identification of *ANKRD11* mutations in KBG syndrome.

In this study, to understand the pathogenic mechanisms underlying the KBG syndrome, we screened *ANKRD11* in additional patients for the documentation of mutation spectrum, studied the cellular characteristics of the wild-type ANKRD11 protein, and analyzed pathogenic variants in humans and *Yoda* mice.

Materials and methods

Patients

Each patient was evaluated by an experienced clinical geneticist to exclude other syndromic forms of ID. Chromosome, fragile X, and microarray studies showed normal results in the affected individuals. The institutional review board at the University of Miami approved this study. All participating individuals provided written informed consent.

Animals

Ankrd11$^{Yod/+}$ or C3H.Cg-Ankrd11 <Yod>/H (EM:00380) congenic on a C3H/HeH genetic background was obtained from the European Mouse Mutant Archive EMMA. The colony was expanded at the University of Miami. At weaning age, *Ankrd11*$^{Yod/+}$ and wild-type littermates were housed 2–4 per cage in a room with a 12-h light/dark cycle with access to food and water ad libitum. All procedures were approved by the University of Miami Institutional Animal Care and followed the NIH Guidelines, "Using Animals in Intramural Research".

Sanger sequencing

Mutations in *ANKRD11* in patients were screened via conventional capillary sequencing. Once a mutation was identified in the proband, available parents were tested for the same variant. Primers were designed to amplify the coding exons and respective flanking intronic regions, along with the 5′ UTR using Primer3 v. 0.4.0 (http://frodo.wi.mit.edu/) and are available upon request. Mouse DNA fragments were amplified using primers F5′-CTGAAGGAGCTGTTCAAGCAA-3′, and R5′-CCTGGCTGCCCGGCAATGAA-3′. 20 ng of genomic DNA was used in conjunction with Betaine (Sigma) and Platinum Taq (Life Technologies) in each PCR reaction. A touchdown protocol was used to amplify target DNA regions. Amplicons were visualized on 2 % agarose gels, and cleanup was conducted using Sephadex. Patient DNA sequencing was obtained using Big Dye Terminator Cycle Sequencing V3.1 Ready Reaction Kit, and ABI PRISM 3130/3730 DNA analyzers (Applied Biosystems). Sequence traces were analyzed with Sequencher 4.7 Software (Gene Codes Corporation). NM_013275.5 was used as reference for nucleotide and codon numbering in humans. In silico analysis to assess disruption of the protein function was performed using Polyphen2 (http://genetics.bwh.harvard.edu/pph2/index.shtml) and Mutation Taster (http://www.mutationtaster.org/).

RT-PCR

Human whole blood samples were collected from the child heterozygous for an *ANKRD11* mutation, unaffected parents, and a control. Total RNA was extracted using PAXgene Blood RNA Kit (Qiagen), and cDNA was synthesized using Superscript III reverse transcriptase

K. Bjørgo
Department of Medical Genetics, Oslo University Hospital, Kirkeveien 166, 0450 Oslo, Norway

A. Lo Castro · P. Curatolo
Department of Neuroscience, Pediatric Neurology and Psychiatry Unit, Tor Vergata University of Rome, 00165 Rome, Italy

(Invitrogen). Nested PCR was performed to amplify a 295-bp region followed by a 218-bp region. Sanger sequencing was used to confirm the presence of the mutation in the RNA. Primers were designed to quantify total *ANKRD11* mRNA (F5′-CAGCCCAGTGGACACAAC-3′ and R5′-CTCTCCACGCTCGTTTCTCT-3′) in the human family heterozygous for a truncating mutation. Additional primer pairs were designed to hybridize directly on the mutation site, where the last two nucleotides on the forward primer matched either the mutant or wild-type allele. Primers designed to anneal to the wild-type DNA were F5′-AAGCCAGTGAGGAAGAGGC-3′ and R5′-TGCTTGGAGTCCTCATATTCG-3′. Primers designed to bind to mutant allele were F5′-TGAAGCCAGTGAGG AAGAGTT-3′ and R5′-TGCTTGGAGTCCTCATATT CG-3′. Amplification of cDNA was completed with a 7900HT Fast Real-Time PCR system (Applied Biosystems). Each reaction was prepared with Syber Green according to the manufacture's protocol (Applied Biosystems). Each condition was performed in triplicate.

Cell culture

MCF-7, MCF-10A and 293T cells were purchased from ATCC and cultured in their recommended media. H1299 cells were cultured in DMEM with 10 % FCS. Neuro2A cells were grown in DMEM medium with 10 % fetal bovine serum, penicillin (100 units/ml), and streptomycin (100 µg/ml) (Gibco by Invitrogen) at 37 °C with 5 % CO_2.

Immunofluorescence analysis

Fibroblasts Primary culture of tail fibroblasts derived from newborn (P0) mice were obtained as previously described (Walz et al. 2003). Fibroblasts derived from wild-type or mutant mice were fixed with PFA 4 % for 15 min followed by permeabilization with PBS-TX100 0.25 %. Detection of Ankrd11 was performed utilizing the rabbit anti-Ankrd11 1/75 (ARP33542, Aviva) and mouse anti-fibrillarin 1/500 (ab4566, Abcam) antibodies. The secondary antibodies utilized were goat anti-rabbit Alexa Fluor 488 (Invitrogen) and goat anti-mouse Alexa Fluor 568 (Invitrogen). To visualize the DNA, DAPI staining was utilized. Images were captured with a LSM710 Zeiss confocal microscope.

ANKRD11 localization during mitosis For the analysis of ANKRD11 localization during mitosis, MCF-7 cells were seeded into Lab-Tek II 4-well chamber slides (Nalge Nunc International, Naperville, IL) and transfected with the pLNCX2-ANKRD11-myc expression construct (Neilsen et al. 2008) using Lipofectamine 2000 (Invitrogen, Carlsbad, CA). Twenty-four hours post-transfection, cells were synchronized in mitosis through incubation with 1 µM nocodazole (Sigma, St Louis, MO) for 16 h. Cells were released from the nocodazole block through three media washes and cultured in fresh media for the indicated time points. Cells were subsequently fixed and permeabilized for immunofluorescence as previously described (Neilsen et al. 2008). Cells were incubated with a mouse anti-myc antibody (Kumar et al. 2005) in 5 % donkey serum (overnight, 4 °C) with subsequent incubation with Alexa Fluor 488-conjugated anti-mouse antibody (Molecular Probes, Eugene, OR) in 5 % donkey serum (1 h, RT). Chomosomes/DNA-rich regions were visualized through initial treatment with RNase A (1 µg/mL, 37 °C, 30 min) and subsequent counterstaining with propidium iodide (100 µg/mL, 37 °C, 30 min) (Sigma, St Louis, MO). Cells were imaged on a BioRad Radiance 2100 Confocal Microscope.

Localization of truncated ANKRD11 protein GFP-ANKRD11 (Neilsen et al. 2008) was digested by *ClaI* and *BamHI*, followed by a filling of the HercII polymerase and a ligation to generate the GFP-ANKRD11$^{1–1,614}$ construct that expresses a truncated *ANKRD11* (1–2,232aa) fused with GFP. The construct sequence was confirmed by Sanger sequencing. Neuro2A cells were transfected with 4.0 µg of the corresponding plasmids using Lipofectamine 2000 (Invitrogen) in 6-well plate with cover slips. Twenty-four hours post-transfection, cells were fixed and immunofluorescence was performed with mouse anti-fibrillarin 1/500 (ab4566, Abcam) antibody as described above.

Western blot analysis

For cell synchronization experiments, MCF-10A cells were blocked at G_1/S phase using a double thymidine block. In brief, sub-confluent cell cultures were grown in the presence of 2 mM thymidine (Sigma, St Louis, MO) for 24 h, subsequently washed in fresh media and cultured without thymidine for an additional 10 h. Cells were then subsequently cultured again in the presence of 2 mM thymidine

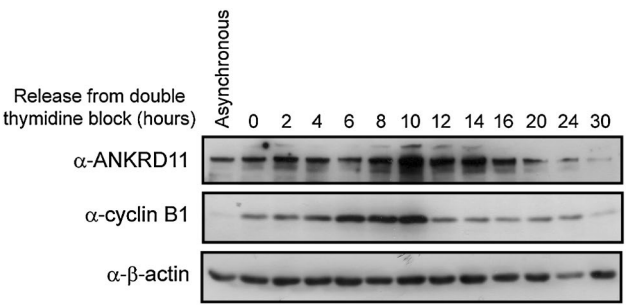

Fig. 1 ANKRD11 is a cell-cycle regulated protein. ANKRD11 protein levels are cell cycle regulated, reaching maximal expression during M phase. MCF-10A cells were synchronized using a double thymidine block, released into fresh media without thymidine and harvested at the indicated time points. ANKRD11, cyclin B1, and beta-actin protein levels were detected using Western blot analysis

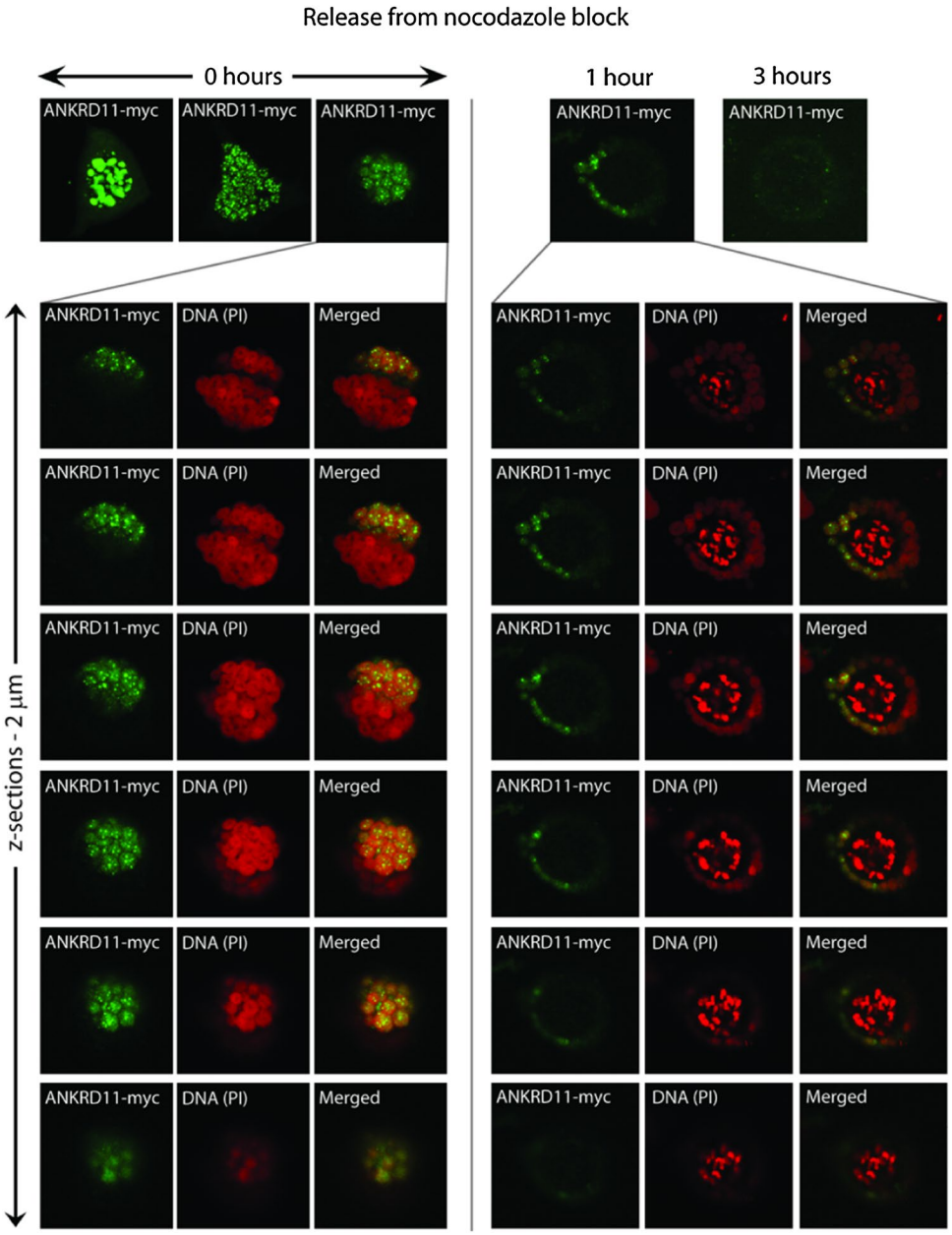

Fig. 2 ANKRD11 localizes to chromatin during mitotic progression and is degraded in late mitosis. MCF-7 cells transiently expressing ANKRD11-myc were blocked in nocodazole (*left* 3 *panels*) or released for the indicated times (*right* 2 *panels*). Cells were immunostained with an α-myc antibody; DNA/chromatin-rich regions were counterstained with propidium iodide (PI) and imaged using confocal microscopy. *Z*-section images of 2 μm thickness were collected for the indicated cells. ANKRD11 localizes to chromatin-rich regions during prometaphase and is degraded in late M phase of the cell cycle (consistent with APC/C-mediated degradation)

for an additional 16 h, thereby synchronizing them in G_1/S phase. Cells were released through two washes in fresh media and collected for Western blot analysis. To assess the cellular compartmentalization of ANKRD11 protein, MCF-10A cells were subjected to subcellular biochemical fractionation as previously described, (Wysocka et al. 2001) followed by Western blot analysis. For ANKRD11 fragment stability assays, H1299 cells were transfected with constructs expressing FLAG-tagged regions of ANKRD11 (Neilsen et al. 2008). Twenty-four hours post-transfection, cells were incubated with either 50 μg/mL cycloheximide (Sigma, St Louis, MO) or vehicle control for a further 16 h followed by collection for Western blot analysis. Western blot analysis was performed as previously described (Neilsen et al. 2008) using the following antibodies; rabbit anti-ANKRD11, mouse anti-FLAG, mouse anti-actin, mouse anti-ORC (Sigma, St Louis, MO), mouse anti-cyclin B1, and rabbit anti-MEK (Neomarkers, Fremont, CA).

Protein-fragment complementation assay (PCA)

The expression constructs encoding the GCN4 protein fused to either the amino (1–158aa) or carboxyl (159–239aa) halves of the YFP proteins were kind gifts from Professor Stephen Michnick. The ANKRD11$^{144–313}$-YFP$^{1–158}$,

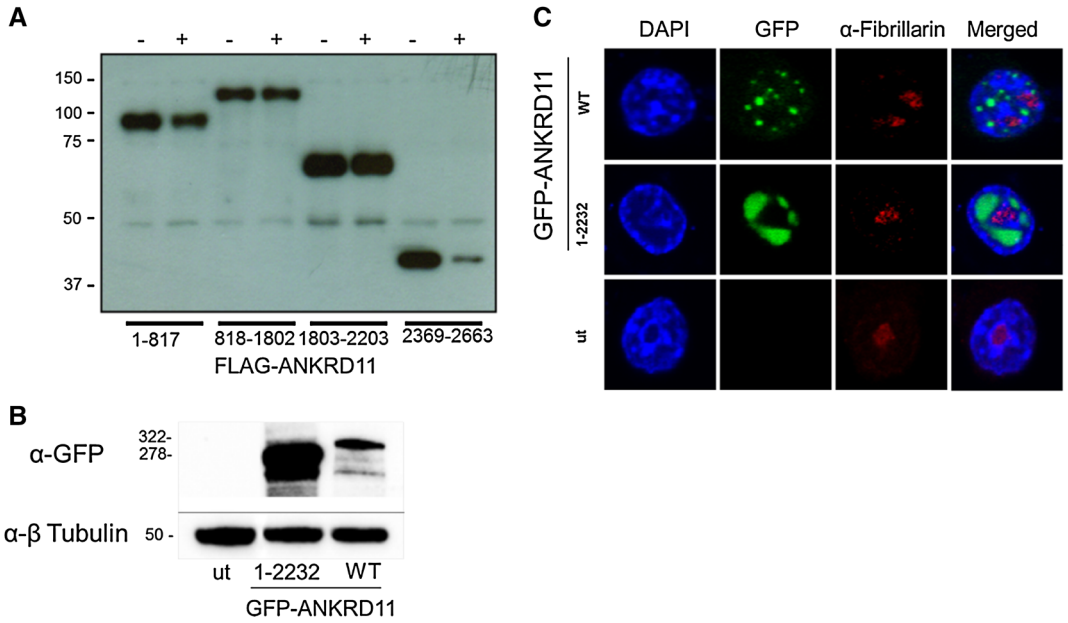

Fig. 3 The C-terminus of ANKRD11 contains the degradation signals. **a** H1299 cells were transfected with constructs expressing FLAG-tagged regions of ANKRD11 as previously reported (Neilsen et al. 2008). Twenty-four hours post-transfection, cells were treated with vehicle control or cycloheximide (50 µg/mL; 16 h) to prevent further protein translation. Western blot analysis demonstrates that the C-terminus region of ANKRD11 (amino acids 2369–2663) is rapidly degraded; however, the other regions of ANKRD11 are not degraded during this time frame. Subcellular localization of the N-terminus ANKRD11 half was detected with an anti-FLAG antibody. **b** Western blot analysis with an anti-GFP antibody of protein extracts derived from the transfections of Neuro-2a cells with the GFP-ANKRD11 WT and GFP-ANKRD11 1-2232 truncated protein plasmids. UT: protein extract from untransfected cells. **c** Immunofluorescence to detect subcellular localization for the wild-type and the ANKRD11 1-2232 truncated protein was performed in transiently transfected Neuro-2a cells. GFP fluorescence was utilized to visualize the subcellular localization and amount of the ANKRD11 proteins. Anti-Fibrillarin antibody (*red*) was utilized to visualize the nucleolus. The nuclei staining was made with DAPI. Untransfected cells in the same slide serve as the untransfected control (color figure online)

ANKRD11$^{144–313}$-YFP$^{159–239}$, p14-YFP$^{1–158}$ and p14-YFP$^{159–239}$ constructs were generated by removing the GCN4 using *NotI* and *ClaI* restriction enzymes and inserting either the p14 ORF (PCRed from MB468 cDNA without a stop codon) or the ANKRD11 region containing the ankyrin domain (429–939 bp), as previously reported (Neilsen et al. 2008). The PCA was performed as previously described (Tarassov et al. 2008). In brief, H1299 or 293T cells were seeded in a 24-well plate and transfected with 400 ng of the indicated ANKRD11$^{144–313}$, GCN4 (positive control) or p14 (negative control) YFP fragment-fusion expression constructs. Twenty-four hours post-transfection, cells were collected in PBS and the total YFP expression levels determined using a FACS Calibur flow cytometer (BD Biosciences). Representative images were collected using an IX51 inverted fluorescent microscope (Olympus).

Statistical analysis

All the experimental data were analyzed using the independent samples *t* test. *P* values lower than 0.05 were considered statistically significant.

Table 1 D-Box positions of the C-terminal region of ANKRD11

D-box #	Human ANKRD11	Mouse Ankrd11
1	RKIL aa2,452–2,455	RKIL aa2,432–2,435
2	**R**GKL aa2,512–2,515	RGKL aa2,492–2,495
3	R**EK**L aa2,523–2,526	REKL aa2,503–2,506

Human C-terminal ANKRD11 was in silico assessed for the presence of D-box motifs. The D-boxes that are conserved in mouse Ankrd11. D-box #2 or #3 is affected by all mutations reported to date in patients with KBG syndrome. Bold letters are 3 amino acids affected by non-truncating mutations. The *Ankrd11^{Yod}* mutation is one amino acid prior to the D-box #3

Results

The abundance of ANKRD11 is tightly regulated during the cell cycle

ANKRD11 has been previously shown to interact with TP53 (MIM191170) and indirectly with CDKN1A (MIM116899), two proteins playing important roles in cell cycle progression (Neilsen et al. 2008). To see if the abundance of ANKRD11 changes during the cell cycle, we

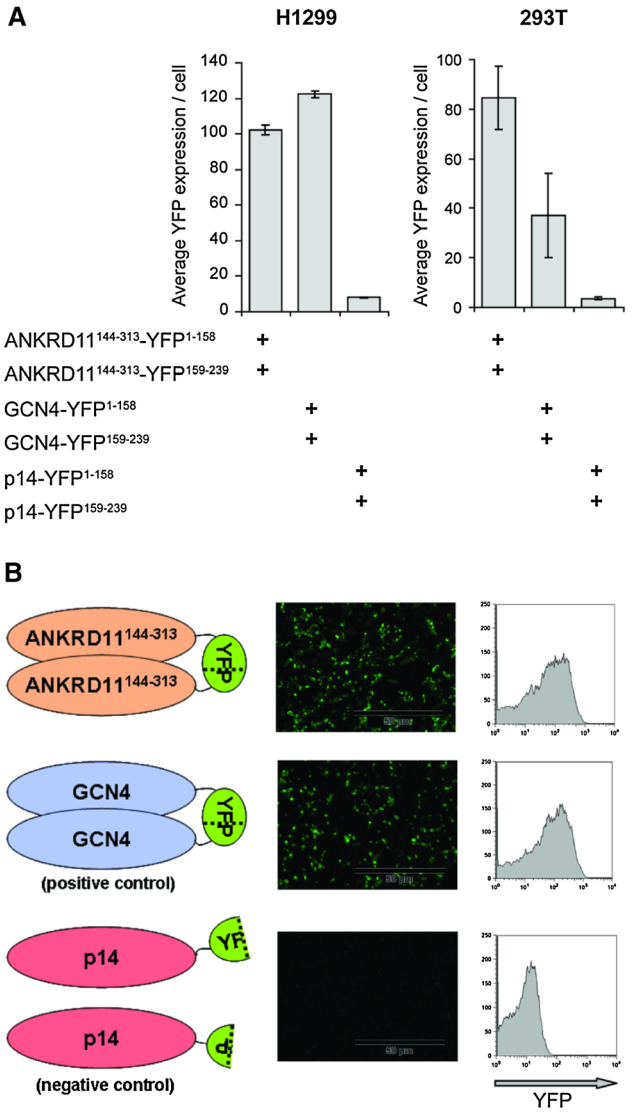

Fig. 4 The ankyrin domain of ANKRD11 homodimerizers. **a** H1299 or 293T cells were transfected with the indicated constructs expressing ANKRD11$^{144–313aa}$ fused to either the amino- or carboxyl-terminal fragments of the YFP protein. Dimerization of the two ANKRD11$^{144–313aa}$ regions was determined by assessing the level of reconstituted YFP expression 24 h post-transfection by flow cytometry. Similar YFP fragment fusions of either GCN4 (a known homodimerizing protein) or p14 (non-dimerizing protein) were used as positive or negative controls, respectively. **b** Representative YFP fluorescent images or flow histograms of H1299 cells (from **a**)

measured the amount of endogenous human ANKRD11 at different stages of the cell cycle. We utilized MCF-10A cells because they have been previously shown to express high levels of endogenous ANKRD11 protein (Neilsen et al. 2008). Cells were synchronized using a double thymidine block, released into fresh media and harvested at different time points. We showed that ANKRD11 levels changed during the cell cycle, similar to those of CCNB1 (MIM123836; cyclin B1), a known cell-cycle regulated protein, reaching maximal expression during M phase as demonstrated by Western blot (Fig. 1). To show the subcellular localization of ANKRD11 during different stages of mitosis, we used nocodazole synchronized cultures of MCF-7 cells (Neilsen et al. 2008), transiently expressing ANKRD11 tagged with myc. ANKRD11-myc was localized to chromatin during chromosomal condensation in prometaphase (Fig. 2). Western blotting of MCF-10A cell fractions also showed that endogenous ANKRD11 was almost exclusively detected in the chromatin-enriched subcellular fraction (Fig. A1). However, the expression of the ANKRD11-myc protein following 3 h release from mitosis (late M phase) was undetectable, suggesting that even the transfected protein is highly unstable during this cell cycle stage.

Degradation signals for ANKRD11 are located at the C-terminus of the protein

To delineate which part of the ANKRD11 protein is signaling the degradation, we generated four constructs to express FLAG-tagged regions of ANKRD11. Twenty hours post-transfection, cells were treated with vehicle or cycloheximide for 16 h to prevent further protein translation. Western blot analysis showed that the C-terminus of ANKRD11 (amino acids 2,369–2,663) is the most rapidly degraded region of ANKRD11 (Fig. 3a). We also generated an N-terminal form of the ANKRD11 protein (ANKRD1$^{1–2,232aa}$) that lacks the C-terminal sequences. The ANKRD11$^{1–2,232aa}$ truncated protein showed a strong accumulation when transfected N2A cells were lysate to be study by Western blot analysis (Fig. 3b) and immunofluorescence (Fig. 3c). One of the most common and well-characterized motifs that direct protein proteolysis is the destruction box (D-box) (Barford 2011). In silico analysis shows that in the C-terminal region of the ANKRD11 there are 3 D-box sequences (Table 1).

N-terminus of ANKRD11 forms homodimers

The N-terminus of ANKRD11 contains an ankyrin domain, which typically provides the interface for protein–protein interactions (Mosavi et al. 2004). Using a yellow fluorescent protein (YFP)-based protein-fragment complementation assay, we demonstrated that the ankyrin domain of ANKRD11 (144–313 amino acids) exists as a homodimer (Fig. 4). Similar levels of homodimerization were observed from the GCN4 leucine zipper protein, which has been previously reported to form dimers and served as a positive control for this assay (Fig. 4).

All *ANKRD11* mutations affect the C-terminus D-boxes

Five *ANKRD11* mutations to cause KBG syndrome were reported in 2011 (Sirmaci et al. 2011). We have since

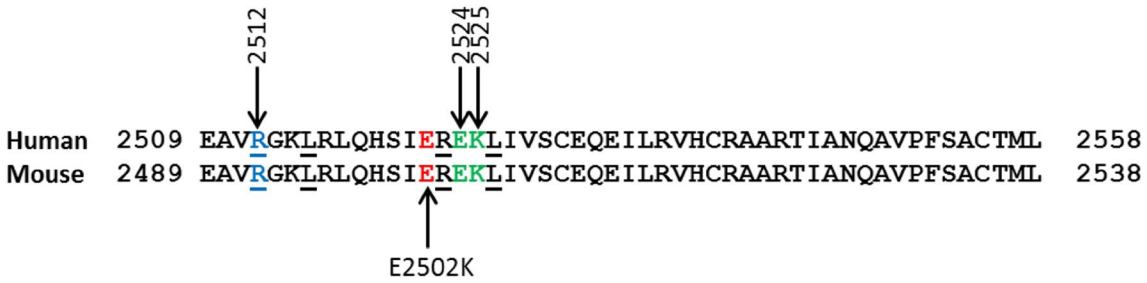

Fig. 5 Schematic representation of ANKRD11 mutations within the C-terminal. Schematic representation of the ANKRD11 mutations in the C-terminal part of the protein for human and mouse is shown. D-box consensus sequences are underlined and in *color* are depicted the mutated aminoacids (color figure online)

identified additional pathogenic *ANKRD11* variants in six cases (Fig. 5; supplemental Figs. A2, A3; Table 2). Nine out of eleven *ANKRD11* mutations lead to premature termination codons at different positions in the gene and the resulting truncated ANKRD11 proteins would lack the C-terminus D-box (Fig. 5). To assess if mRNA produced with these mutations is stable, we studied patient A with a truncating mutation that is located in the 5′ end of the gene (p.R595_A2663delinsS). Sanger sequencing of cDNA obtained from a peripheral blood mRNA sample showed the presence of the mutant allele, suggesting that a complete nonsense-mediated mRNA decay is not triggered (Fig. A3a). This finding was corroborated by quantitative analysis, which excluded nonsense-mediated decay in the proband (Fig. A3a). One reported mutation is a splice site variant that causes the deletion of the two central amino acids of a C-terminus D-box consensus sequence (**R**XX**L**) (Fig. 5; Table 1) (Barbaric et al. 2008). The mutation identified in patient F constitutes the sole missense *ANKRD11* variant associated with KBG syndrome up to date. Coincidentally, the p.R2512Q mutation changes the R from a D-box contiguous to the final C-terminus D-box. Thus, our analysis shows that the two C-terminus D-boxes are affected by all mutations reported to date in humans.

Mouse *Yoda* mutation adjacent to a D-box affects protein degradation

In silico analysis showed that the mutated amino acid of Ankrd11 in the *Yoda* mouse is just one amino acid upstream of the syntenic last C-terminus D-box in humans (Fig. 5). This suggests that the degradation of Ankrd11 is disrupted. Therefore, we assessed the accumulation of the endogenous wild-type and mutant protein in primary culture of tail fibroblasts. In fibroblasts derived from wild-type mice, the protein localized in nuclear speckles as reported earlier (Neilsen et al. 2008). However, *Ankrd11*$^{Yod/+}$ derived fibroblasts showed accumulation (Fig. 6a, b). To understand if this phenotype could be related to the abnormal degradation of the protein by the proteasome we subsequently studied the localization of the wild-type Ankrd11 protein when the proteasome was inhibited. The exposure of wild-type fibroblasts to inhibitor MG132 induced the accumulation of the wild-type Ankrd11 (Fig. 6c, d) suggesting that the proteasome is indeed related to Ankrd11 degradation.

Discussion

Here, we report that the pathogenesis of KBG syndrome, a condition characterized by syndromic ID with behavioral abnormalities, is related to impaired degradation of ANKRD11. We showed that wild-type ANKRD11 is tightly regulated through the cell cycle.

We show here that the C-terminus region of the ANKRD11 protein is critical for regulation of its degradation. Interestingly enough three D-box sequences were found in this portion of the protein, with 100 % of homology between the human and the mouse sequence. Two of them were found to be disrupted in KBG patients and in the *Yoda* mouse, strongly suggesting that they play a role in the molecular cause of the phenotype.

The ubiquitin–proteasome system regulates neuronal migration, neuritogenesis, and the formation and elimination of synapses (Kawabe and Brose 2011). Thus, disruption of this system can cause neuronal dysfunction and lead to neurological disease and ID. (Tai and Schuman 2008) Mendelian forms of ubiquitin–proteasome pathway dysfunction have so far included disorders where mutations affect the core components of the system, potentially involving multiple target proteins. A prototype disorder is Angelman syndrome (MIM105830) in which mutations in UBE3A (MIM601623) encoding the ubiquitin ligase E3A are causative. Angelman syndrome is characterized by ID, speech delay, gait ataxia, seizures, and distinctive behavior.

The ubiquitin–proteasome is a mechanism present in eukaryotic cells to regulate biological transitions through protein destruction (Hershko and Ciechanover 1998).

Table 2 Clinical findings observed in patients with *ANKRD11* mutations

Patients	A	B	C	D	E	F	Total in 11 *ANKRD11* mutations[a]
Mutation	c.1785_1786delGCinsTT (p. R595_A2663delinsSer)	c.1903_1907delAAACA (p.K635Qfs*26)	c.2130delG (p.W710Cfs*9)	c.4283_4286delAAGA (p.K1428Ifs*13)	c.6817_6833delGGCCCCGCCCCGAACAC (p.G2273Cfs*17)	c.7535G>A (p.R2512Q)	See Fig. 5
Mutation is de novo	+	N/A	N/A	N/A	+	+	7/8
Sex (M/F)	F	M	M	M	M	M	10/1
Age (years)	15	13	26	15	15	13	7–50
General findings							
Short stature[b]	+	+	−	+	+	−	8/11 (73 %)
Developmental delay/ID[b]	+	+	+	−[c]	+	+	10/11 (91 %)
Craniofacial findings[b]							
Brachycephaly/turricephaly	+	+	+	−	+	+	10/11 (91 %)
Distinct shape of face (round or triangular)	+	+	+	+	+	+	11/11 (100 %)
Wide eyebrows/synophrys	+	+	+	+	+	+	10/11 (91 %)
Hypertelorism	−	−	−	−	−	+	5/11 (45 %)
Ptosis	−	−	+	−	−	+	6/11 (55 %)
Anteverted nostrils	+	+	+	+	+	+	11/11 (100 %)
Prominent nasal bridge	+	+	+	+	+	+	11/11 (100 %)
Dental findings							
Macrodontia of upper central permanent incisors[b]	+	+	+	+	+	+	11/11 (100 %)
Oligodontia	−	−	−	+	−	+	6/10 (60 %)
Skeletal abnormalities							
Abnormal vertebrae[b]	N/A	+	+	N/A	+	+	5/7 (71 %)
Cervical ribs[b]	N/A	−	−	N/A	−	−	2/9 (22 %)
Delayed bone age[b]	+	+	N/A	+	N/A	N/A	5/5 (100 %)
Short tubular bones of hands[b]	−	+	+	N/A	N/A	+	7/8 (87 %)
Other							
Abnormal EEG/seizures[b]	−	−	−	−	−	−	1/8 (12 %)
Syndactyly of toes	−	−	−	−	−	+	3/11 (27 %)
5th finger clinodactyly[b]	+	−	+	−	−	−	7/11 (64 %)
Cryptorchidism	N/A	−	−	−	+	−	5/10 (50 %)

N/A Not available

[a] Mutations reported here and those published in Handrigan et al. (2013)

[b] Diagnostic criterion suggested in Brancati et al. (2006)

[c] While testing showed normal intelligence in patient D, he had Asperger syndrome, attention deficit disorder, speech delay, and dyslexia

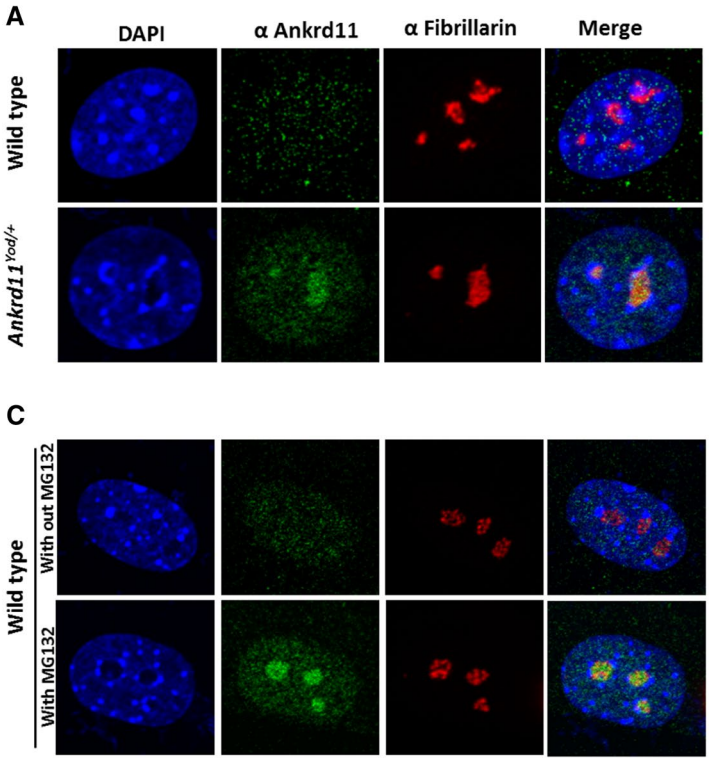

Ankrd11 Nucleolus Accumulation	Yes	No	Total Cell count
Wild type	9 +/- 1.2	91 +/- 1.2	100
Ankrd11 $^{Yoda/+}$	90 +/- 1.5	10 +/- 1.5	100

WT Ankrd11 Nucleolus Accumulation	Yes	No	Total Cell count
- MG132	9 +/- 1.2	91 +/- 1.2	100
+ MG132	92 +/- 0.8	8 +/- 0.8	100

Fig. 6 *Ankrd11*^{Yod} shows abnormal accumulation that can be mimicked by inhibition of the proteasome. **a** Immunofluorescence was performed in primary cultured fibroblast derived from WT or *Ankrd11*$^{Yod/+}$ mice with an anti-ANKRD11 antibody (in *green*), and with anti-Fibrillarin antibody (*red*) to visualize the nucleolus. The nuclei staining was made with DAPI. **b** Table depicts the quantification of the subcellular localization for 200 cells. An *N* of 3 independent animals was utilized in these experiments. **c** Immunofluorescence was performed in primary cultured fibroblast derived from WT mice treated or not treated with a proteasome inhibitor drug, MG132, in the culture media. Anti-ANKRD11 antibody (in *green*) and anti-fibrillarin antibody (*red*) were utilized. The nuclei staining was made with DAPI. **d** Table depicts the quantification of the subcellular localization for 200 cells. An *N* of 3 independent animals was utilized in these experiments (color figure online)

Ubiquitination of a target protein that needs a ubiquitin-activating enzyme (E1), a conjugating enzyme (E2), and a ubiquitin ligase (E3). The polyubiquitinated substrate is then degraded by the proteasome. APC/C is an E3 ubiquitin ligase that controls mitosis and G1 by targeting different substrates for degradation by the 26S proteasome. The D-box is the most common sequence known to target substrates to the APC/C complex (Barford 2011).

While several deletions on the long arm of chromosome 16 involving *ANKRD11* have been reported to cause a phenotype overlapping with KBG syndrome, only five cases had deletions limited to *ANKRD11* without including neighboring genes (Isrie et al. 2012; Khalifa et al. 2013; Spengler et al. 2013). In two of these cases (Isrie et al. 2012; Khalifa et al. 2013), the deletions were predicted to leave the 5′ end of *ANKRD11* intact, which would lead to the production of a truncated protein missing C-terminus D-boxes. The remaining three cases had variable short stature, craniofacial anomalies, behavioral problems or mild ID. Since the abundance of ANKRD11 is tightly controlled during the cell cycle, it is likely that haploinsufficiency is enough to produce a clinical phenotype. However, our findings show that ANKRD11 forms homodimers through its N-terminus, which remains intact in all known *ANKRD11* mutations. This suggests that the pathogenesis of a heterozygous ANKRD11 mutant may involve a dominant-negative mechanism containing a dimer with wild-type ANKRD11.

In summary, we show that the abundance of ANKRD11 is regulated during the cell cycle and that ANKRD11 variants lacking the C-terminus D-boxes are at the heart of the phenotype seen in KBG syndrome. Understanding the mechanism of cognitive impairment and behavioral problems in ANKRD11-mutated individuals holds the potential of targeted therapeutic strategies.

Acknowledgments We thank Karen Neagley for the administrative support and the English proofreading of the manuscript, Professor Stephen Michnick for the PCA expression constructs, and Dr. Raman Sharma for his useful discussions. This work was partially funded by the Hayward Foundation and NHMRC Project Grant APP1009452.

Conflict of interest The authors declare no conflict of interest.

References

Barbaric I, Perry MJ, Dear TN, Rodrigues Da Costa A, Salopek D, Marusic A, Hough T, Wells S, Hunter AJ, Cheeseman M, Brown SD (2008) An ENU-induced mutation in the Ankrd11 gene results in an osteopenia-like phenotype in the mouse mutant Yoda. Physiol Genomics 32:311–321. doi:10.1152/physiolgenomics.00116.2007

Barford D (2011) Structure, function and mechanism of the anaphase promoting complex (APC/C). Q Rev Biophys 44:153–190. doi:10.1017/S0033583510000259

Brancati F, Sarkozy A, Dallapiccola B (2006) KBG syndrome. Orphanet J Rare Dis 1:50. doi:10.1186/1750-1172-1-50

Handrigan GR, Chitayat D, Lionel AC, Pinsk M, Vaags AK, Marshall CR, Dyack S, Escobar LF, Fernandez BA, Stegman JC, Rosenfeld JA, Shaffer LG, Goodenberger M, Hodge JC, Cain JE, Babul-Hirji R, Stavropoulos DJ, Yiu V, Scherer SW, Rosenblum ND (2013) Deletions in 16q24.2 are associated with autism spectrum disorder, intellectual disability and congenital renal malformation. J Med Genet 50:163–173. doi:10.1136/jmedgenet-2012-101288

Herrmann J, Pallister PD, Tiddy W, Opitz JM (1975) The KBG syndrome-a syndrome of short stature, characteristic facies, mental retardation, macrodontia and skeletal anomalies. Birth Defects Orig Artic Ser 11:7–18

Hershko A, Ciechanover A (1998) The ubiquitin system. Annu Rev Biochem 67:425–479

Isrie M, Hendriks Y, Gielissen N, Sistermans EA, Willemsen MH, Peeters H, Vermeesch JR, Kleefstra T, Van Esch H (2012) Haploinsufficiency of ANKRD11 causes mild cognitive impairment, short stature and minor dysmorphisms. Eur J Hum Genet 20:131–133. doi:10.1038/ejhg.2011.105

Kawabe H, Brose N (2011) The role of ubiquitylation in nerve cell development. Nat Rev Neurosci 12(5):251–268

Khalifa M, Stein J, Grau L, Nelson V, Meck J, Aradhya S, Duby J (2013) Partial deletion of ANKRD11 results in the KBG phenotype distinct from the 16q24.3 microdeletion syndrome. Am J Med Genet A 161A:835–840. doi:10.1002/ajmg.a.35739

Kumar R, Neilsen PM, Crawford J, McKirdy R, Lee J, Powell JA, Saif Z, Martin JM, Lombaerts M, Cornelisse CJ, Cleton-Jansen AM, Callen DF (2005) FBXO31 is the chromosome 16q24.3 senescence gene, a candidate breast tumor suppressor, and a component of an SCF complex. Cancer Res 65:11304–11313. doi:10.1158/0008-5472.CAN-05-0936

Marshall CR, Noor A, Vincent JB, Lionel AC, Feuk L, Skaug J, Shago M, Moessner R, Pinto D, Ren Y, Thiruvahindrapduram B, Fiebig A, Schreiber S, Friedman J, Ketelaars CE, Vos YJ, Ficicioglu C, Kirkpatrick S, Nicolson R, Sloman L, Summers A, Gibbons CA, Teebi A, Chitayat D, Weksberg R, Thompson A, Vardy C, Crosbie V, Luscombe S, Baatjes R, Zwaigenbaum L, Roberts W, Fernandez B, Szatmari P, Scherer SW (2008) Structural variation of chromosomes in autism spectrum disorder. Am J Hum Genet 82:477–488. doi:10.1016/j.ajhg.2007.12.009

Miyatake S, Murakami A, Okamoto N, Sakamoto M, Miyake N, Saitsu H, Matsumoto N (2013) A de novo deletion at 16q24.3 involving ANKRD11 in a Japanese patient with KBG syndrome. Am J Med Genet A 161A:1073–1077. doi:10.1002/ajmg.a.35661

Mosavi LK, Cammett TJ, Desrosiers DC, Peng ZY (2004) The ankyrin repeat as molecular architecture for protein recognition. Protein Sci 13:1435–1448. doi:10.1110/ps.03554604

Neilsen PM, Cheney KM, Li CW, Chen JD, Cawrse JE, Schulz RB, Powell JA, Kumar R, Callen DF (2008) Identification of ANKRD11 as a p53 coactivator. J Cell Sci 121:3541–3552. doi:10.1242/jcs.026351

Sacharow S, Li D, Fan YS, Tekin M (2012) Familial 16q24.3 microdeletion involving ANKRD11 causes a KBG-like syndrome. Am J Med Genet A 158A:547–552. doi:10.1002/ajmg.a.34436

Sirmaci A, Spiliopoulos M, Brancati F, Powell E, Duman D, Abrams A, Bademci G, Agolini E, Guo S, Konuk B, Kavaz A, Blanton S, Digilio MC, Dallapiccola B, Young J, Zuchner S, Tekin M (2011) Mutations in ANKRD11 cause KBG syndrome, characterized by intellectual disability, skeletal malformations, and macrodontia. Am J Hum Genet 89:289–294. doi:10.1016/j.ajhg.2011.06.007

Skjei KL, Martin MM, Slavotinek AM (2007) KBG syndrome: report of twins, neurological characteristics, and delineation of diagnostic criteria. Am J Med Genet A 143:292–300. doi:10.1002/ajmg.a.31597

Spengler S, Oehl-Jaschkowitz B, Begemann M, Hennes P, Zerres K, Eggermann T (2013) Haploinsufficiency of ANKRD11 (16q24.3) is not obligatorily associated with cognitive impairment but shows a clinical overlap with Silver–Russell syndrome. Mol Syndromol 4:246–249. doi:10.1159/000351765

Tai HC, Schuman EM (2008) Ubiquitin, the proteasome and protein degradation in neuronal function and dysfunction. Nat Rev Neurosci 11:826–838

Tarassov K, Messier V, Landry CR, Radinovic S, Serna Molina MM, Shames I, Malitskaya Y, Vogel J, Bussey H, Michnick SW (2008) An in vivo map of the yeast protein interactome. Science 320:1465–1470. doi:10.1126/science.1153878

Walz K, Caratini-Rivera S, Bi W, Fonseca P, Mansouri DL, Lynch J, Vogel H, Noebels JL, Bradley A, Lupski JR (2003) Modeling del(17)(p11.2p11.2) and dup(17)(p11.2p11.2) contiguous gene syndromes by chromosome engineering in mice: phenotypic consequences of gene dosage imbalance. Mol Cell Biol 23:3646–3655

Willemsen MH, Fernandez BA, Bacino CA, Gerkes E, de Brouwer AP, Pfundt R, Sikkema-Raddatz B, Scherer SW, Marshall CR, Potocki L, van Bokhoven H, Kleefstra T (2010) Identification of ANKRD11 and ZNF778 as candidate genes for autism and variable cognitive impairment in the novel 16q24.3 microdeletion syndrome. Eur J Hum Genet 18:429–435. doi:10.1038/ejhg.2009.192

Wysocka J, Reilly PT, Herr W (2001) Loss of HCF-1-chromatin association precedes temperature-induced growth arrest of tsBN67 cells. Mol Cell Biol 21:3820–3829. doi:10.1128/MCB.21.11.3820-3829.2001

Zhang A, Yeung PL, Li CW, Tsai SC, Dinh GK, Wu X, Li H, Chen JD (2004) Identification of a novel family of ankyrin repeats containing cofactors for p160 nuclear receptor coactivators. J Biol Chem 279:33799–33805. doi:10.1074/jbc.M403997200

Zhang A, Li CW, Chen JD (2007) Characterization of transcriptional regulatory domains of ankyrin repeat cofactor-1. Biochem Biophys Res Commun 358:1034–1040. doi:10.1016/j.bbrc.2007.05.017